Modeling Atmospheric Transport of Cosmogenic Radionuclide ^{10}Be Using GEOS-Chem 14.1.1 and ECHAM6.3-HAM2.3: Implications for Solar and Geomagnetic Reconstructions

Minjie Zheng, Florian Adolphi, Sylvaine Ferrachat, Florian Mekhaldi, Zhengyao Lu, Andreas Nilsson, Ulrike Lohmann

Geophysical Research Letters

RESEARCH LETTER
10.1029/2023GL106642

Modeling Atmospheric Transport of Cosmogenic Radionuclide ^{10}Be Using GEOS-Chem 14.1.1 and ECHAM6.3-HAM2.3: Implications for Solar and Geomagnetic Reconstructions

Minjie Zheng[1,2], Florian Adolphi[3,4], Sylvaine Ferrachat[1], Florian Mekhaldi[2,5], Zhengyao Lu[6], Andreas Nilsson[2], and Ulrike Lohmann[1]

[1]Institute for Atmospheric and Climate Science, ETH Zürich, Zürich, Switzerland, [2]Department of Geology, Lund University, Lund, Sweden, [3]Alfred Wegener Institute, Helmholtz Centre for Polar and Marine Research, Bremerhaven, Germany, [4]Faculty of Geosciences, Bremen University, Bremen, Germany, [5]Aix Marseille University, CNRS, IRD, INRAE, CEREGE, Aix-en-Provence, France, [6]Department of Physical Geography and Ecosystem Science, Lund University, Lund, Sweden

Abstract A prerequisite to applying ^{10}Be in natural archives for solar and geomagnetic reconstructions is to know how ^{10}Be deposition reflects atmospheric production changes. However, this relationship remains debated. To address this, we use two state-of-the-art global models GEOS-Chem and ECHAM6.3-HAM2.3 with the latest beryllium production model. During solar modulation, both models suggest that ^{10}Be deposition reacts proportionally to global production changes, with minor latitudinal deposition biases (<5%). During geomagnetic modulation, however, ^{10}Be deposition changes are enhanced by ∼15% in the tropics and attenuated by 20%–35% in subtropical and polar regions compared to global production changes. Such changes are also hemispherically asymmetric, attributed to asymmetric production between hemispheres. For the solar proton event in 774/5 CE, ^{10}Be shows a 15% higher deposition increase in polar regions than in tropics. This study highlights the importance of atmospheric mixing when comparing ^{10}Be from different locations or to independent geomagnetic field records.

Plain Language Summary The cosmogenic radionuclide beryllium-10 (^{10}Be) deposition in natural archives can be used to reconstruct solar and geomagnetic changes in the past. Understanding how ^{10}Be deposition reflects atmospheric production rate changes is crucial for these applications. However, this relationship remains debated. To address this issue, we use two state-of-the-art global models, GEOS-Chem 14.1.1 and ECHAM6.3-HAM2.3, along with the latest beryllium production model (CRAC: Be). When responding to solar modulation, both models indicate that ^{10}Be deposition corresponds proportionally to global production rate changes, with a minor latitudinal bias. However, during geomagnetic modulation, ^{10}Be deposition changes significantly compared to global production rate changes. ^{10}Be deposition also shows varying hemispheric responses to geomagnetic modulation, attributed to the asymmetric production between hemispheres. For the extreme solar proton event in 774/5 CE, ^{10}Be shows a higher deposition flux increase in the polar regions compared to the tropics. These findings underscore the need to account for atmospheric mixing on ^{10}Be deposition from different locations, especially for the changes due to the geomagnetic field variations.

Key Points:

- We used two state-of-the-art global models incorporating the latest beryllium production rates to study the sources of ^{10}Be deposition
- ^{10}Be deposition shows strong regional bias compared to the global signal in response to geomagnetic modulation but not to solar modulation
- ^{10}Be deposition shows varying hemispheric responses to geomagnetic modulation, attributed to the asymmetric production between hemispheres

Supporting Information:

Supporting Information may be found in the online version of this article.

Correspondence to:

M. Zheng,
minjie.zheng@geol.lu.se

Citation:

Zheng, M., Adolphi, F., Ferrachat, S., Mekhaldi, F., Lu, Z., Nilsson, A., & Lohmann, U. (2024). Modeling atmospheric transport of cosmogenic radionuclide ^{10}Be using GEOS-Chem 14.1.1 and ECHAM6.3-HAM2.3: Implications for solar and geomagnetic reconstructions. *Geophysical Research Letters*, *51*, e2023GL106642. https://doi.org/10.1029/2023GL106642

Received 5 OCT 2023
Accepted 9 JAN 2024

Author Contributions:

Conceptualization: Minjie Zheng
Data curation: Minjie Zheng, Florian Mekhaldi
Formal analysis: Minjie Zheng, Florian Adolphi, Andreas Nilsson, Ulrike Lohmann
Funding acquisition: Minjie Zheng
Investigation: Minjie Zheng, Ulrike Lohmann

1. Introduction

Cosmogenic radionuclides (e.g., ^{10}Be) from ice cores are indirect proxies to reconstruct paleo-solar (e.g., Bard et al., 2000; Muscheler et al., 2007) and geomagnetic variations (e.g., Zheng et al., 2021). ^{10}Be (half-life of 1.38 million years, Chmeleff et al., 2010) is mainly produced in the atmosphere by interactions between galactic cosmic ray fluxes (GCRs) and atmospheric atoms (Lal & Peters, 1967). The GCR fluxes are modulated by solar and geomagnetic fields before reaching Earth's atmosphere. Hence, atmospheric production rates of ^{10}Be are related to solar and geomagnetic field variability. Additionally, a small amount of ^{10}Be (<1%) is produced by solar cosmic rays that originate from the Sun (Vogt et al., 1990). However, extreme solar proton events (SPEs) can produce relatively energetic and large particle fluxes resulting in large increases in atmospheric ^{10}Be production (e.g., Mekhaldi et al., 2015). About two-thirds of ^{10}Be is produced in the stratosphere while the rest is produced in the troposphere (Poluianov et al., 2016). After production, ^{10}Be mainly attaches to sulfate aerosols,

Methodology: Minjie Zheng, Florian Adolphi, Sylvaine Ferrachat, Florian Mekhaldi, Zhengyao Lu, Ulrike Lohmann
Resources: Minjie Zheng, Sylvaine Ferrachat, Zhengyao Lu, Ulrike Lohmann
Software: Sylvaine Ferrachat, Zhengyao Lu
Supervision: Ulrike Lohmann
Validation: Minjie Zheng
Writing – original draft: Minjie Zheng
Writing – review & editing: Minjie Zheng, Florian Adolphi, Sylvaine Ferrachat, Florian Mekhaldi, Zhengyao Lu, Andreas Nilsson, Ulrike Lohmann

gets transported with them, and is eventually deposited in different natural archives (e.g., ice cores) mainly through wet deposition (Alley et al., 1995; Delaygue et al., 2015).

Reconstructing past solar and geomagnetic field changes from ^{10}Be deposition relies on the assumption that ^{10}Be deposition variability is proportional to atmospheric production changes (e.g., Muscheler et al., 2016; Zheng et al., 2021). However, this relationship is not well understood as atmospheric ^{10}Be production rates are spatially heterogeneous with a strong altitude and latitude dependence (Poluianov et al., 2016). There is a long-standing debate on whether polar ^{10}Be deposition reflects global or local production signals (e.g., Adolphi et al., 2023; Bard et al., 1997; Pedro et al., 2012; Steig et al., 1996). Some studies assumed that polar ^{10}Be deposition mainly originates from polar regions and introduced a "polar enhancement coefficient" to account for the higher solar modulation influence at high latitudes (e.g., Bard et al., 1997; Steig et al., 1996). However, this assumption has been challenged (e.g., Heikkilä et al., 2009; Muscheler et al., 2007). Heikkilä et al. (2009) argued that the majority of polar ^{10}Be (60%–70%) comes from the stratosphere where ^{10}Be is well mixed due to the long residence time (1–2 years), hence the polar ^{10}Be should reflect the global production signal. Adolphi et al. (2023) recently proposed that in polar regions, the solar modulation signal in ^{10}Be is only enhanced by less than 10% compared to the global signal, whereas the geomagnetic signal is attenuated by up to 37%.

Two general circulation models (GCMs), GISS ModelE (Field et al., 2006), and ECHAM5-HAM (Heikkilä, Beer, Jouzel, et al., 2008; Heikkilä et al., 2009) have been applied to investigate this "polar bias" debate. However, so far, no agreement has been reached. By using GISS ModelE, Field et al. (2006) reported a 20% enhancement in polar ^{10}Be deposition compared to a global average change during reduced solar modulation (from 700 to 500 MeV), and a 20% decrease during a reduction of the geomagnetic field strength. In contrast, Heikkilä et al. (2009) found no significant polar bias regarding geomagnetic modulation using ECHAM5-HAM.

To answer the question of whether the ^{10}Be deposition is proportional to global or local production signals, it is necessary to understand the sources of ^{10}Be deposition. To the best of our knowledge, there is only one study by Heikkilä et al. (2009) with the ECHAM5-HAM model (denoted as the H09 mixing scenario) tracing the production in the stratosphere, tropical troposphere, subtropical troposphere, and polar troposphere individually. The results may be model-dependent and need to be investigated using different models. Furthermore, they used the old production model by Masarik and Beer (1999) without accounting for contributions from alpha and heavier particles. Finally, they assumed ^{10}Be is well mixed in the stratosphere and traced the stratospheric ^{10}Be production as one source box. Thus the H09 mixing scenario does not allow an investigation of potential preservation of hemispherical production differences in deposition due to large-scale geomagnetic field asymmetries (Panovska et al., 2023).

This study aims to improve the interpretation of ^{10}Be deposition using two state-of-the-art global models: ECHAM6.3-HAM2.3 aerosol-climate model, and GEOS-Chem 14.1.1 atmospheric transport model. Both GEOS-Chem and ECHAM-HAM have been demonstrated to be able to simulate ^{10}Be transport and deposition reasonably well (e.g., Heikkilä, Beer, Jouzel, et al., 2008; Zheng et al., 2023). Models are incorporated with the latest ^{10}Be production model CRAC: Be (Cosmic Ray Atmospheric Cascade: application to Beryllium) by Poluianov et al. (2016). The main goals are (a) to quantify the contribution of ^{10}Be produced in different regions of the atmosphere to the ^{10}Be deposition at different latitudes and whether this is model dependent; (b) to solve the debate of whether ^{10}Be deposition at different latitudes reacts proportionally to the global production rate changes, in response to the solar/geomagnetic modulations and extreme SPEs.

2. Models and Data

2.1. GEOS-Chem 14.1.1 and ECHAM6.3-HAM2.3

GEOS-Chem 14.1.1 (denoted as GEOS-Chem) is a chemical transport model driven by archived meteorological data sets, either from the outputs of GCMs (e.g., Murray et al., 2021) or assimilated meteorological data sets archived from the Goddard Earth Observing System (e.g., MERRA2, Gelaro et al., 2017). The model assumes that ^{10}Be behaves as a submicron aerosol after production and is removed by dry and wet depositions (Liu et al., 2001; Zheng et al., 2023). The wet deposition scheme includes rainout (in-cloud scavenging), scavenging in convective updrafts (Mari et al., 2000), and washout (below-cloud scavenging) by precipitation (Wang et al., 2011). Dry deposition is based on the resistance-in-series scheme of Wesely (1989). The simulations are conducted with a horizontal resolution of 2° × 2.5° and 72 vertical levels up to 0.01 hPa. We use the MERRA2

meteorological reanalysis data set (Gelaro et al., 2017), which is re-gridded to the model resolution to drive GEOS-Chem.

ECHAM-HAM is a combination of the global climate model ECHAM (Stevens et al., 2013) with the aerosol microphysics module HAM (Stier et al., 2005). The HAM module includes the microphysical processes, the emission and deposition (wet, dry, and sedimentation) of aerosols, a sulfur chemistry scheme, and aerosol impact radiation (Stier et al., 2005). ^{10}Be has been simulated in an old version of ECHAM-HAM (ECHAM5-HAM) (e.g., Heikkilä, Beer, & Feichter, 2008; Heikkilä, Beer, Jouzel, et al., 2008). Here we use the latest version ECHAM6.3-HAM2.3 (denoted as E63H23, Neubauer et al., 2019; Tegen et al., 2019) with a similar configuration of ^{10}Be as in ECHAM5-HAM. The ^{10}Be is assumed to be transported similarly to sulfate aerosols and its deposition is calculated as proportional to those of sulfate aerosols. Specifically, for dry deposition and sedimentation, an area-weighted averaged velocity of sulfate aerosols is used. For the wet deposition, ^{10}Be is scavenged with the same efficiency as that of sulfate aerosols. We use the middle-atmospheric configuration with 47 vertical levels up to 80 km, and a spectral resolution of T63, corresponding to 1.875° × 1.875° horizontal resolution. E63H23 experiments are free runs to align with the previous study by Heikkilä et al. (2009). Furthermore, a comparison between the free-running E63H23 and GEOS-Chem driven by the reanalysis data enables us to assess whether our conclusions are influenced by the set-up of free simulations.

2.2. Box Source Tracing and Box Mixing Model

To investigate the sources of ^{10}Be deposition, the atmosphere is divided into 12 source regions corresponding to latitudinal bands of 30° for the stratosphere and troposphere, respectively. This classification is based on atmospheric circulation cells and latitudinal distribution of ^{10}Be production rates (e.g., Adolphi et al., 2023). Classification of stratospheric and tropospheric components is based on the tropopause pressure in models. A previous study has suggested that ECHAM5 suffers from a tropopause pressure bias in the polar regions in free simulations (Santer et al., 2003). Indeed, E63H23 experiments underestimate the tropopause pressure over the polar regions compared to the MERRA2 reanalysis data, leading to a higher classification of polar tropospheric ^{10}Be in E63H23 (Figure S1 in Supporting Information S1).

The ^{10}Be transport and deposition characteristics derived from E63H23 and GEOS-Chem can be simplified into a 12-box mixing model, which implicitly accounts for the transport and deposition influences on ^{10}Be deposition (e.g., Adolphi et al., 2023). The deposition concentration in the j deposition box (D_j) could be expressed as follows:

$$D_j = \sum_{i=1}^{12} M_{ij} \times C_{ij}$$

Where M_{ij} and C_{ij} are the mixing ratio and the latitudinal weighted production rates of the box i for the deposition box j. Here the atmospheric production rates are divided into 12 boxes. The ^{10}Be production rates used in the box mixing model are discussed in Text S1 in Supporting Information S1.

2.3. Production Model

The ^{10}Be production rates are calculated using the latest production model: CRAC: Be model (Poluianov et al., 2016) with the local interstellar spectrum and solar modulation from Herbst et al. (2017). The geomagnetic cutoff rigidity is taken from Copeland (2018). For the Maunder simulation, we use a constant solar modulation function of 200 MeV (e.g., Heikkilä, Beer, & Feichter, 2008). For the Laschamps simulation, we use a constant solar modulation function of 500 MeV and the spatial cut-off rigidity generated by the geomagnetic field model LSMOD.2 at 40.95 ka (Gao et al., 2022).

2.4. Experiments Set-Up

The overview of simulations is shown in Table S1 in Supporting Information S1. We first run simulations over the period 1999–2013 with present solar modulation (Herbst et al., 2017) and geomagnetic cut-off rigidity (Copeland, 2018) (referred as control). Additionally, to evaluate the deposition bias due to solar and geomagnetic modulations, we further run two sensitivity simulations with the same climate conditions but different production

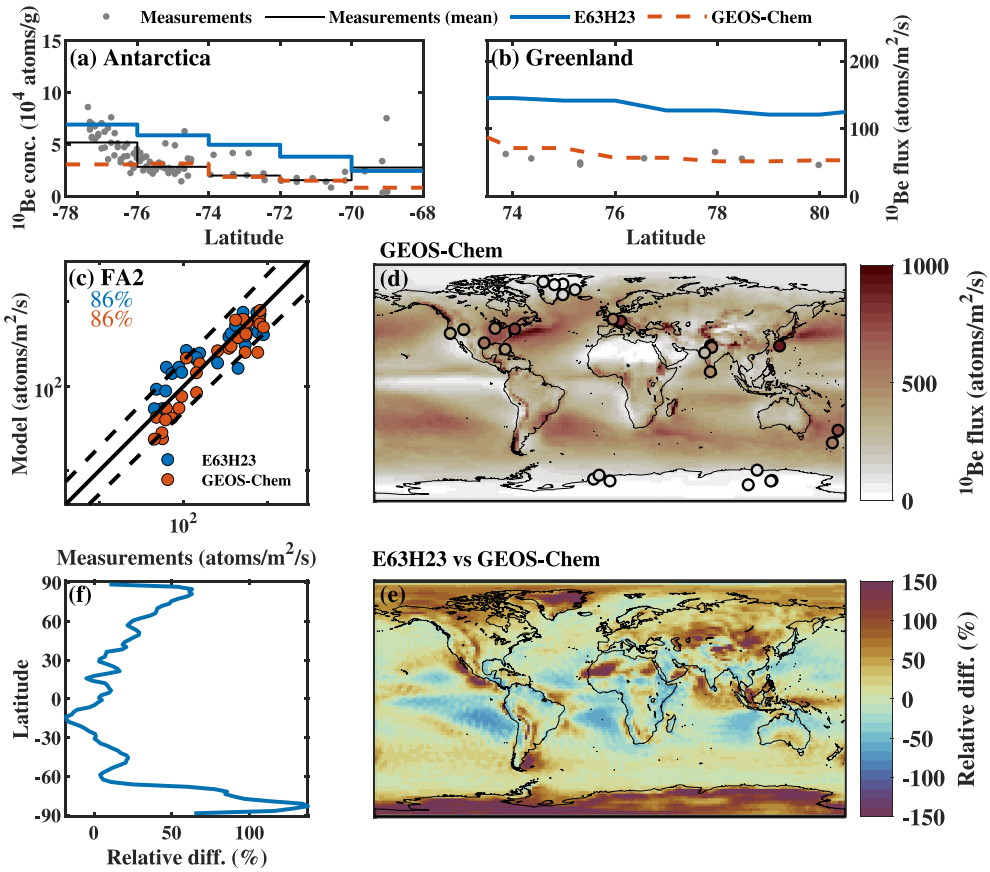

Figure 1. Comparison between modeled ^{10}Be outputs from GEOS-Chem and E63H23 averaged over the period 2005–2013 and measurements from (a) Antarctica traverse, (b) Greenland traverse, and (c) a compiled deposition flux data set. Panel (d) shows GEOS-Chem deposition fluxes averaged over 2005–2013 overplotted with measurements (color-coded dots) from panel (c). Panel (e) shows the relative differences of modeled ^{10}Be deposition flux (calculated as (E63H23/GEOS-Chem-1) × 100%) over the period 2005–2013 while the zonal mean of relative differences is shown in panel (f). For the Antarctica traverse, the model data are plotted as the latitudinal band (2-degree) based on measurement sites. ^{10}Be concentrations are calculated using the ^{10}Be fluxes multiplied by the ice density and then divided by corresponding accumulation rates. For the Greenland traverse, the model lines are plotted as a function of latitudes averaged over the Greenland region. FA2 indicates the percentages of model data within the factor of 2.

corresponding to a solar minimum (Maunder minimum) and a geomagnetic minimum (Laschamps excursions) (Figure S2 in Supporting Information S1). For all simulations, the first 6 years are used for model spin-up (e.g., Heikkilä, Beer, & Feichter, 2008; Zheng et al., 2023) to make sure ^{10}Be reaches equilibrium in the atmosphere and the remaining 9 years are used for analysis. We compared stratospheric ^{10}Be concentration within the simulations with constant production rates (e.g., Laschamps simulation), in which the drift in stratospheric ^{10}Be concentrations is below 2% per year.

We also simulated ^{7}Be with both models for the control simulation. ^{7}Be is commonly used to validate the model's ability to simulate beryllium as it shares the same transport and deposition process as ^{10}Be but with more measurements available for validation (e.g., Field et al., 2006; Heikkilä, Beer, & Feichter, 2008). ^{7}Be production rates are calculated using the same production model and set-up as ^{10}Be.

3. Results and Discussions

3.1. Model Validation

The model ^{10}Be results are compared with the ^{10}Be deposition data set compiled by Zheng et al. (2023) and two ice ^{10}Be traverse data sets from East Antarctica (Horiuchi et al., 2022) and Greenland (Heikkilä, Beer, & Feichter, 2008) (Figure 1). While the model ^{7}Be results are compared with air and deposition measurements

compiled by Zhang et al. (2021) (Figure S3 in Supporting Information S1). Most measurements cover several years and do not necessarily cover the same period as the simulation period. Hence, we mainly focus on evaluating whether the models can reproduce measurements instead of discussing which model performs better.

Both models show good agreements with ^{7}Be and ^{10}Be measurements within a factor of 2 (Figure 1 and Figure S3 in Supporting Information S1). Discrepancies are larger for ^{7}Be deposition flux than for surface air concentrations due to several reasons (Zhang et al., 2021): (a) observations for the deposition usually cover shorter periods compared to the surface air samples; (b) the model resolution may be still too coarse to capture the local precipitation at some sites which can influence the deposition flux. The increasing trend of the Antarctic traverse ^{10}Be from coastal Antarctica to inland Antarctica is captured by both models (Figure 1a). GEOS-Chem shows a good agreement with the Greenland traverse deposition, while E63H23 shows much higher values (approximately 100% higher) (Figure 1b). Generally, E63H23 shows a higher ^{10}Be deposition (about 50%–100%) over the polar regions compared to GEOS-Chem (Figures 1e and 1f). This cannot be explained by the precipitation differences as E63H23 shows lower precipitation over the polar regions compared to GEOS-Chem, hence lower scavenging rates of ^{10}Be (Figure S4 in Supporting Information S1). Another explanation could be due to the higher classification of tropospheric ^{10}Be production in E63H23 compared to GEOS-Chem (more than 50%; Figure S1 in Supporting Information S1), hence more locally produced ^{10}Be is deposited in polar regions. For a detailed discussion of models' abilities capturing beryllium transport and deposition processes, we refer to studies by Zheng et al. (2023) for GEOS-Chem and Heikkilä, Beer, and Feichter (2008) for ECHAM-HAM.

3.2. Atmospheric Mixing and Stratospheric Fractions of ^{10}Be

3.2.1. Stratospheric and Tropospheric Contributions to ^{10}Be Deposition

Figure 2 and Table S2 in Supporting Information S1 show the sink fraction of the 30° tropospheric and stratospheric production bands at different latitudes. In GEOS-Chem simulations, the tropical tropospheric ^{10}Be is mostly (75%–80%) deposited in the tropics. ^{10}Be produced in both the polar and the subtropical latitudes are mostly deposited in the subtropical regions (55%–65%). The majority of stratospheric ^{10}Be (>90%) is deposited in the tropical and subtropical regions. The model also shows that ^{10}Be in the stratosphere is not mixed entirely which is different from a previous study by Heikkilä et al. (2009). Less than 15% of stratospheric ^{10}Be produced in the polar and subtropical regions is deposited in the opposite hemisphere. In polar and subtropical regions, there is a gradient of increased stratospheric contribution to local deposition with latitudes. Despite different setups in E63H23 and GEOS-Chem, E63H23 shows similar mixing features to those of GEOS-Chem, even though the deposition values for each box vary slightly (mostly <5%; see Table S2 and Figure S5 in Supporting Information S1).

Both models show that the stratospheric contribution is dominant in the deposition flux, about 60%–61% (GEOS-Chem) and 54%–58% (E63H23) in the polar regions, and 63%–66% (GEOS-Chem) and 61%–65% (E63H23) in the subtropical and tropical regions (Figure 2). E63H23 shows a slightly lower stratospheric contribution in polar regions than GEOS-Chem, which is attributed to the higher classification of tropospheric ^{10}Be production in E63H23 (see Section 2.2).

3.2.2. Changes of ^{10}Be Deposition Due To Solar and Geomagnetic Modulations

Here we simplify the derived mixing scenarios into a 12-box model (see Section 2.2 for details) to evaluate the relative deposition change in response to solar and geomagnetic modulations (here referred to sensitivity) (Figure 3). The results of sensitivity to solar and geomagnetic modulations are rather similar for E63H23 and GEOS-Chem: enhanced/attenuated up to 5% regarding the solar modulation and up to 35% regarding geomagnetic modulation, respectively. In response to solar modulation changes, ^{10}Be deposition in different latitudes varies proportionally to the globally averaged signal and does not show strong deposition biases (less than 5%). This agrees with previous studies showing no strong solar enhancement of ^{10}Be deposition in polar regions (e.g., Adolphi et al., 2023; Pedro et al., 2012).

However, the box mixing model demonstrates a clear deposition bias corresponding to geomagnetic modulation (Figures 3a–3c). For the tropical regions, the reduced geomagnetic modulation can lead to an enhancement of the local ^{10}Be deposition change up to 15% compared to the global change of ^{10}Be production. For the subtropical and polar regions instead, an attenuation of up to 35% is observed. The deposition also shows different hemispheric

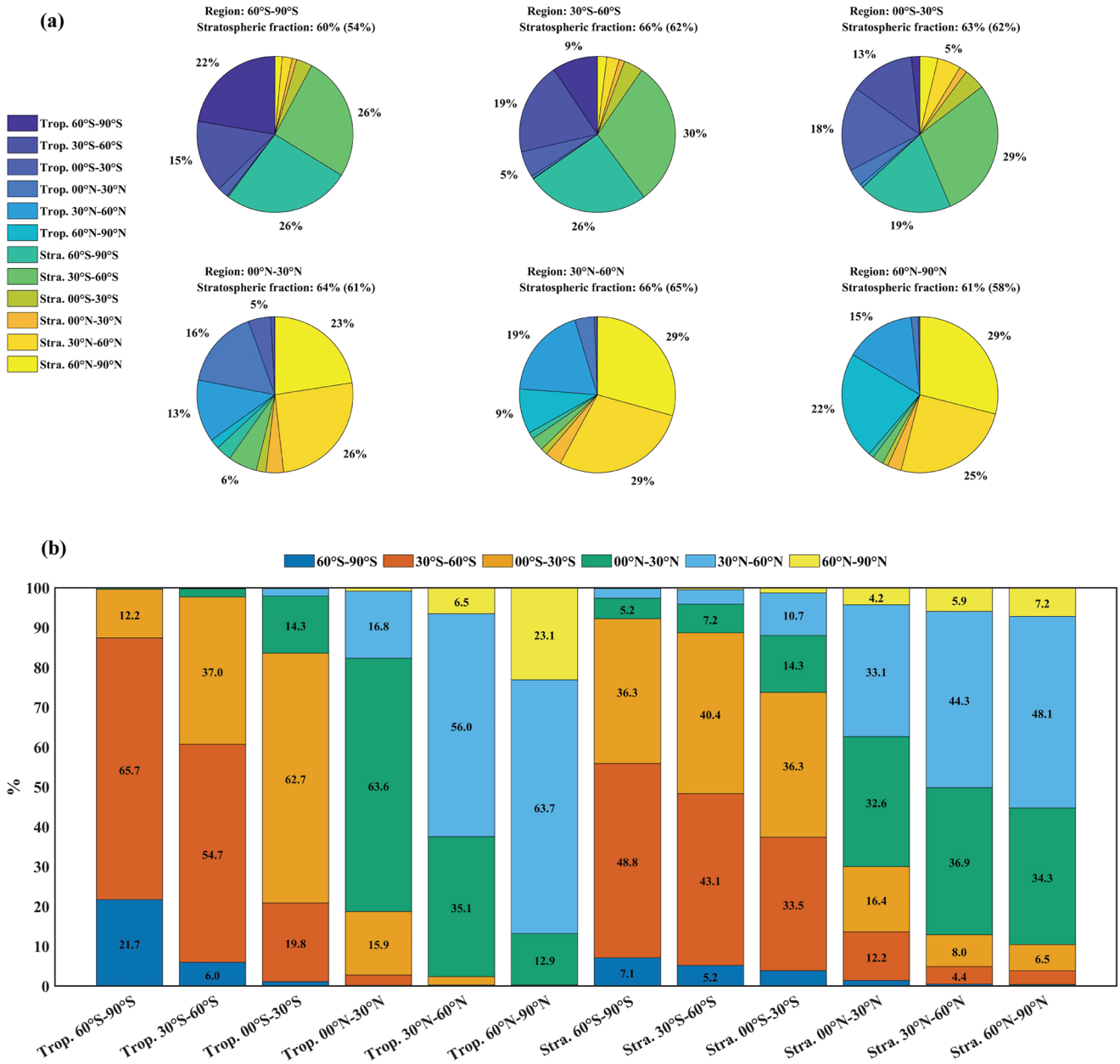

Figure 2. (a) The sources of ^{10}Be deposition and (b) sink fraction of ^{10}Be production in different regions modeled from GEOS-Chem averaged over 2005–2013. The stratospheric contributions in bracket in panel (a) are from the E63H23 simulation. Only values larger than 4% are labeled.

responses to the geomagnetic modulation (up to 10%) due to a persistent hemispheric asymmetry in production rates leading to larger amplitude variations in Northern Hemisphere (Panovska et al., 2023). This asymmetric deposition signal in polar regions is not shown using the H09 mixing scenario from Heikkilä et al. (2009) (Figure S6 in Supporting Information S1) as they simply consider the stratosphere source as one well-mixed box that mitigates the asymmetric production signal.

The mixing model results (including the H09 mixing scenario) disagree with the ECHAM5 simulation by Heikkilä et al. (2009) which suggested no strong polar bias for the Laschamps experiment. We further investigate two experiments simulating a solar and a geomagnetic field intensity minimum to evaluate this deposition bias. The simulations show that, indeed, the relative increase in ^{10}Be deposition is latitudinally dependent due to the latitudinal difference in production combined with significant (but incomplete) mixing across the latitudes (Figure 4). Especially for the geomagnetic minimum scenario, the atmospheric mixing is not strong enough to

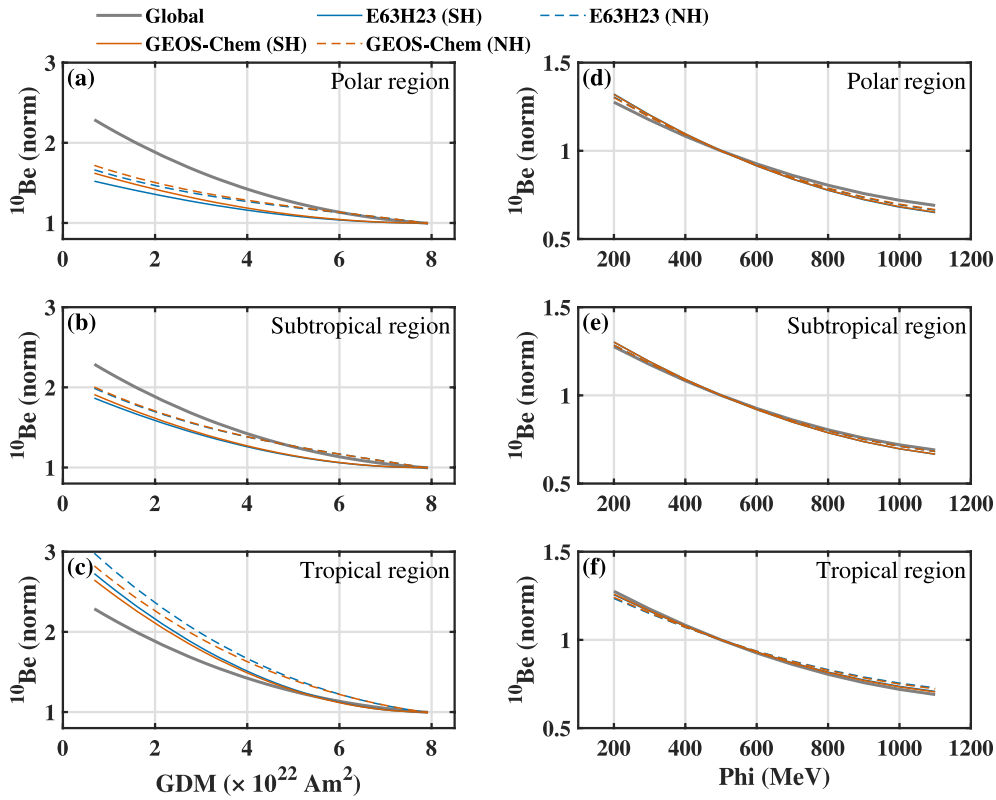

Figure 3. Simulated deposition changes for different mixing scenarios as a function of solar modulation function (Phi) and geomagnetic dipole moment. All ^{10}Be fluxes are normalized over the Phi of 500 MeV and GMD of 7.8 × 10^{22} Am^2. The "SH" and "NH" indicate the southern hemisphere and northern hemisphere, respectively.

homogenize the latitudinal production rate patterns for the geomagnetic modulation which leads to a 250%–650% increase over the tropical regions (Figure S2f in Supporting Information S1).

The results from global climate models and box mixing model reasonably agree with the measurements which show significant differences in deposition increase related to the Laschamps excursions (Figure 4d). ^{10}Be from polar ice cores show about a 75% increase during the Laschamps event. In comparison, ^{10}Be measurements from marine sediments agree well with the global signal as they are usually well mixed due to the long residence time of ^{10}Be in the ocean (about 200–1,000 years depending on locations). The "non-polar bias" result shown by Heikkilä et al. (2009) could be due to the old production model (Masarik & Beer, 1999) used in ECHAM5-HAM which are less sensitive to the geomagnetic modulation in comparison to the recently updated ^{10}Be production model (Elsässer et al., 2015).

3.2.3. Enhancement Factor of ^{10}Be Deposition for an Extreme Solar Proton Event in 774/5 CE

Finally, we apply the 12-box mixing model to evaluate the enhancement factor of ^{10}Be due to the extreme SPE in 774/5 CE (denoted as SPE775, Mekhaldi et al., 2015; Miyake et al., 2012). The details of ^{10}Be production rates for SPE775 are shown in Text S1 in Supporting Information S1. The model enhancement factor is calculated as the relatively increase in ^{10}Be deposition compared to the annual average ^{10}Be deposition flux in the absence of SPEs (with a solar modulation of 525 MeV and the same geomagnetic dipole moment value).

The model enhancement factors (about 2.9–3 for E63H23 and GEOS-Chem) agree with the factors inferred from ice core measurements (3 ± 0.3) (Mekhaldi et al., 2021) (Figure S7 in Supporting Information S1). This agreement is better than the global or H09 mixing scenarios (2.65–2.7) which consider the well-mixed stratospheric ^{10}Be. The results suggest that the ^{10}Be resulting from SPE events is sensitive to the mixing of stratospheric ^{10}Be and that ice core measurements can be expected to provide a slight overestimate of the global enhancement factor. Interestingly, Paleari et al. (2022) instead reported a 17% lower enhancement factor from ice core ^{10}Be compared to tree-ring ^{14}C, which is assumed to be better mixed in the atmosphere. This mismatch may indicate remaining uncertainties in the production yield functions of both isotopes.

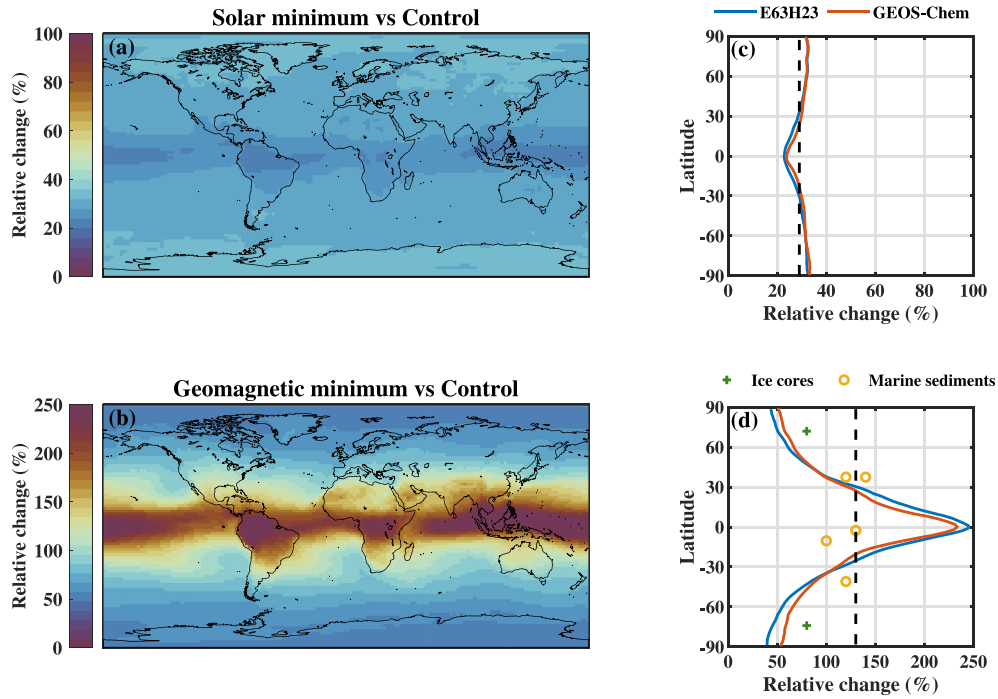

Figure 4. GEOS-Chem modeled relative changes of ^{10}Be deposition for the (a) solar minimum and (b) geomagnetic minimum compared to the control simulation and the corresponding zonal mean (c, d). The black dashed lines in panel (c, d) indicate the ones considering global mixing. The green crosses and orange circles indicate the relative changes inferred from measurements in ice cores and marine sediments (Adolphi et al., 2023).

4. Conclusions

Here we applied two state-of-the-art global models GEOS-Chem 14.1.1 (denoted as GEOS-Chem) and ECHAM6.3-HAM2.3 (denoted as E63H23) with the latest beryllium production model (CRAC: Be) to solve a longstanding debate: how changes in ^{10}Be deposition reflect changes in its atmospheric production rate. The model simulations agree reasonably with ^{7}Be and ^{10}Be measurements.

Despite their different setups, GEOS-Chem and E63H23 both show similar mixing features for ^{10}Be. Most tropospheric and stratospheric ^{10}Be (>70%) is deposited within the same hemisphere of its production. Stratospheric contributions dominate ^{10}Be deposition (54%–66%). E63H23 shows a slightly lower stratospheric contribution for the polar regions (54%–58%) compared to GEOS-Chem (60%–61%). This is due to the underestimated polar tropopause in E63H23, resulting in an overestimate of polar tropospheric ^{10}Be.

We further simplified the outputs of the global model experiments into a 12-box mixing model, which allows an estimation of relative ^{10}Be deposition changes under user-defined solar or geomagnetic modulations. For changes in solar modulation, ^{10}Be deposition mainly reflects the global averaged production signals without showing a strong regional bias. However, during geomagnetic field changes, ^{10}Be deposition shows a strong regional bias (15%–35%). This is because the atmospheric mixing is insufficient to homogenize the large latitudinal differences in ^{10}Be production rates associated with geomagnetic field changes. These findings are further supported by global model simulations and measurements from ice cores and marine sediments. Due to non-dipolar components of the geomagnetic field, the deposition also shows different hemispheric responses (~10%) to the geomagnetic modulation.

Finally, the mixing model suggests there is a regional deposition bias for SPE in 774/5 CE which leads to an enhancement factor of 2.9–3 in the polar regions compared to a global mean enhancement factor of 2.7.

Overall, this study shows the importance of atmospheric mixing when comparing ^{10}Be from different locations or independent geomagnetic field records, especially during periods of low geomagnetic field intensity. The mixing scenarios derived in this study can be used in future studies to explicitly account for the transport and deposition influence on the ^{10}Be.

Data Availability Statement

The model outputs can be accessed in the public repository in Zheng et al. (2024).

Acknowledgments
This project is supported by the Swedish Research Council (Dnr: 2021-06649) granted to M. Zheng. F. Adolphi acknowledges funding through the Helmholtz Association (VH-NG 1501). A. Nilsson and F. Mekhaldi acknowledge funding from the Swedish Research Council (2020-04813 and 2020-00420). Z. Lu acknowledges Swedish Research Council Vetenskapsrådet (Grant 2022-03617) and FORMAS mobility (Grant 2020-02267). The GEOS-Chem model is managed by the Atmospheric Chemistry Modeling Group at Harvard University. GEOS-Chem support team at Harvard University and Washington University in St. Louis (WashU) is acknowledged for their effort. GEOS-Chem input files were obtained from the GEOS-Chem Data Portal enabled by WashU. The ECHAM–HAMMOZ model is developed by a consortium composed of ETH Zurich, the Max Planck Institute for Meteorology, Forschungszentrum Juelich, the University of Oxford, the Finnish Meteorological Institute, and the Leibniz Institute for Tropospheric Research; it is managed by the Center for Climate Systems Modeling (C2SM) at ETH Zurich.

References

Adolphi, F., Herbst, K., Nilsson, A., & Panovska, S. (2023). On the polar bias in ice core ^{10}Be data. *Journal of Geophysical Research: Atmospheres*, *128*(4), e2022JD038203. https://doi.org/10.1029/2022jd038203

Alley, R., Finkel, R., Nishiizumi, K., Anandakrishnan, S., Shuman, C., Mershon, G., et al. (1995). Changes in continental and sea-salt atmospheric loadings in central Greenland during the most recent deglaciation: Model-based estimates. *Journal of Glaciology*, *41*(139), 503–514. https://doi.org/10.3189/S0022143000034845

Bard, E., Raisbeck, G., Yiou, F., & Jouzel, J. (2000). Solar irradiance during the last 1200 years based on cosmogenic nuclides. *Tellus B: Chemical and Physical Meteorology*, *52*(3), 985–992. https://doi.org/10.1034/j.1600-0889.2000.d01-7.x

Bard, E., Raisbeck, G. M., Yiou, F., & Jouzel, J. (1997). Solar modulation of cosmogenic nuclide production over the last millennium: Comparison between ^{14}C and ^{10}Be records. *Earth and Planetary Science Letters*, *150*(3), 453–462. https://doi.org/10.1016/S0012-821X(97)00082-4

Chmeleff, J., von Blanckenburg, F., Kossert, K., & Jakob, D. (2010). Determination of the ^{10}Be half-life by multicollector ICP-MS and liquid scintillation counting. *Nuclear Instruments and Methods in Physics Research Section B: Beam Interactions with Materials and Atoms*, *268*(2), 192–199. https://doi.org/10.1016/j.nimb.2009.09.012

Copeland, K. (2018). CARI-7 documentation: Geomagnetic cutoff rigidity calculations and tables for 1965-2010 (DOT/FAA/AM-19/04). Retrieved from https://rosap.ntl.bts.gov/view/dot/57079

Delaygue, G., Bekki, S., & Bard, E. (2015). Modelling the stratospheric budget of beryllium isotopes. *Tellus B: Chemical and Physical Meteorology*, *67*(1), 28582. https://doi.org/10.3402/tellusb.v67.28582

Elsässer, C., Wagenbach, D., Levin, I., Stanzick, A., Christl, M., Wallner, A., et al. (2015). Simulating ice core ^{10}Be on the glacial–interglacial timescale. *Climate of the Past*, *11*(2), 115–133. https://doi.org/10.5194/cp-11-115-2015

Field, C. V., Schmidt, G. A., Koch, D., & Salyk, C. (2006). Modeling production and climate-related impacts on ^{10}Be concentration in ice cores. *Journal of Geophysical Research*, *111*(D15), D15107. https://doi.org/10.1029/2005jd006410

Gao, J., Korte, M., Panovska, S., Rong, Z., & Wei, Y. (2022). Effects of the Laschamps excursion on geomagnetic cutoff rigidities. *Geochemistry, Geophysics, Geosystems*, *23*(2), e2021GC010261. https://doi.org/10.1029/2021GC010261

Gelaro, R., McCarty, W., Suárez, M. J., Todling, R., Molod, A., Takacs, L., et al. (2017). The modern-era retrospective analysis for Research and applications, version 2 (MERRA-2). *Journal of Climate*, *30*(14), 5419–5454. https://doi.org/10.1175/JCLI-D-16-0758.1

Heikkilä, U., Beer, J., & Feichter, J. (2008). Modeling cosmogenic radionuclides ^{10}Be and ^{7}Be during the maunder minimum using the ECHAM5-HAM general circulation model. *Atmospheric Chemistry and Physics*, *8*(10), 2797–2809. https://doi.org/10.5194/acp-8-2797-2008

Heikkilä, U., Beer, J., & Feichter, J. (2009). Meridional transport and deposition of atmospheric ^{10}Be. *Atmospheric Chemistry and Physics*, *9*(2), 515–527. https://doi.org/10.5194/acp-9-515-2009

Heikkilä, U., Beer, J., Jouzel, J., Feichter, J., & Kubik, P. (2008). ^{10}Be measured in a GRIP snow pit and modeled using the ECHAM5-HAM general circulation model. *Geophysical Research Letters*, *35*(5), L05817. https://doi.org/10.1029/2007gl033067

Herbst, K., Muscheler, R., & Heber, B. (2017). The new local interstellar spectra and their influence on the production rates of the cosmogenic radionuclides ^{10}Be and ^{14}C. *Journal of Geophysical Research: Space Physics*, *122*(1), 23–34. https://doi.org/10.1002/2016ja023207

Horiuchi, K., Kato, S., Ohtani, K., Kurita, N., Tsutaki, S., Nakazawa, F., et al. (2022). Spatial variations of ^{10}Be in surface snow along the inland traverse route of Japanese Antarctic Research Expeditions. *Nuclear Instruments and Methods in Physics Research Section B: Beam Interactions with Materials and Atoms*, *533*, 61–65. https://doi.org/10.1016/j.nimb.2022.10.018

Lal, D., & Peters, B. (1967). Cosmic ray produced radioactivity on the Earth. In K. Sitte (Ed.), *Kosmische Strahlung II/cosmic rays II* (pp. 551–612). Springer Berlin Heidelberg.

Liu, H., Jacob, D. J., Bey, I., & Yantosca, R. M. (2001). Constraints from ^{210}Pb and ^{7}Be on wet deposition and transport in a global three-dimensional chemical tracer model driven by assimilated meteorological fields. *Journal of Geophysical Research*, *106*(D11), 12109–12128. https://doi.org/10.1029/2000jd900839

Mari, C., Jacob, D. J., & Bechtold, P. (2000). Transport and scavenging of soluble gases in a deep convective cloud. *Journal of Geophysical Research*, *105*(D17), 22255–22267. https://doi.org/10.1029/2000JD900211

Masarik, J., & Beer, J. (1999). Simulation of particle fluxes and cosmogenic nuclide production in the Earth's atmosphere. *Journal of Geophysical Research*, *104*(D10), 12099–12111. https://doi.org/10.1029/1998jd200091

Mekhaldi, F., Adolphi, F., Herbst, K., & Muscheler, R. (2021). The signal of solar storms embedded in cosmogenic radionuclides: Detectability and uncertainties. *Journal of Geophysical Research: Space Physics*, *126*(8), e2021JA029351. https://doi.org/10.1029/2021ja029351

Mekhaldi, F., Muscheler, R., Adolphi, F., Aldahan, A., Beer, J., McConnell, J. R., et al. (2015). Multiradionuclide evidence for the solar origin of the cosmic-ray events of 774/5 and 993/4. *Nature Communications*, *6*(1), 8611. https://doi.org/10.1038/ncomms9611

Miyake, F., Nagaya, K., Masuda, K., & Nakamura, T. (2012). A signature of cosmic-ray increase in AD 774-775 from tree rings in Japan. *Nature*, *486*(7402), 240–242. https://doi.org/10.1038/nature11123

Murray, L. T., Leibensperger, E. M., Orbe, C., Mickley, L. J., & Sulprizio, M. (2021). GCAP 2.0: A global 3-D chemical-transport model framework for past, present, and future climate scenarios. *Geoscientific Model Development*, *14*(9), 5789–5823. https://doi.org/10.5194/gmd-14-5789-2021

Muscheler, R., Adolphi, F., Herbst, K., & Nilsson, A. (2016). The revised sunspot record in comparison to cosmogenic radionuclide-based solar activity reconstructions. *Solar Physics*, *291*(9–10), 3025–3043. https://doi.org/10.1007/s11207-016-0969-z

Muscheler, R., Joos, F., Beer, J., Müller, S. A., Vonmoos, M., & Snowball, I. (2007). Solar activity during the last 1000yr inferred from radionuclide records. *Quaternary Science Reviews*, *26*(1–2), 82–97. https://doi.org/10.1016/j.quascirev.2006.07.012

Neubauer, D., Ferrachat, S., Siegenthaler-Le Drian, C., Stier, P., Partridge, D. G., Tegen, I., et al. (2019). The global aerosol–climate model ECHAM6.3–HAM2.3 – Part 2: Cloud evaluation, aerosol radiative forcing, and climate sensitivity. *Geoscientific Model Development*, *12*(8), 3609–3639. https://doi.org/10.5194/gmd-12-3609-2019

Paleari, C. I., Mekhaldi, F., Adolphi, F., Christl, M., Vockenhuber, C., Gautschi, P., et al. (2022). Cosmogenic radionuclides reveal an extreme solar particle storm near a solar minimum 9125 years BP. *Nature Communications*, *13*(1), 214. https://doi.org/10.1038/s41467-021-27891-4

Panovska, S., Poluianov, S., Gao, J., Korte, M., Mishev, A., Shprits, Y. Y., & Usoskin, I. (2023). Effects of global geomagnetic field variations over the past 100,000 years on cosmogenic radionuclide production rates in the Earth's atmosphere. *Journal of Geophysical Research: Space Physics*, *128*(8), e2022JA031158. https://doi.org/10.1029/2022JA031158

Pedro, J. B., McConnell, J. R., van Ommen, T. D., Fink, D., Curran, M. A. J., Smith, A. M., et al. (2012). Solar and climate influences on ice core ^{10}Be records from Antarctica and Greenland during the neutron monitor era. *Earth and Planetary Science Letters*, *355–356*, 174–186. https://doi.org/10.1016/j.epsl.2012.08.038

Poluianov, S. V., Kovaltsov, G. A., Mishev, A. L., & Usoskin, I. G. (2016). Production of cosmogenic isotopes ^{7}Be, ^{10}Be,^{14}C, ^{22}Na, and ^{36}Cl in the atmosphere: Altitudinal profiles of yield functions. *Journal of Geophysical Research: Atmospheres*, *121*(13), 8125–8136. https://doi.org/10.1002/2016jd025034

Santer, B. D., Sausen, R., Wigley, T. M. L., Boyle, J. S., AchutaRao, K., Doutriaux, C., et al. (2003). Behavior of tropopause height and atmospheric temperature in models, reanalyses, and observations: Decadal changes. *Journal of Geophysical Research*, *108*(D1), ACL1-1–ACL1-22. https://doi.org/10.1029/2002JD002258

Steig, E. J., Polissar, P. J., Stuiver, M., Grootes, P. M., & Finkel, R. C. (1996). Large amplitude solar modulation cycles of ^{10}Be in Antarctica: Implications for atmospheric mixing processes and interpretation of the ice core record. *Geophysical Research Letters*, *23*(5), 523–526. https://doi.org/10.1029/96gl00255

Stevens, B., Giorgetta, M., Esch, M., Mauritsen, T., Crueger, T., Rast, S., et al. (2013). Atmospheric component of the MPI-M Earth System model: ECHAM6. *Journal of Advances in Modeling Earth Systems*, *5*(2), 146–172. https://doi.org/10.1002/jame.20015

Stier, P., Feichter, J., Kinne, S., Kloster, S., Vignati, E., Wilson, J., et al. (2005). The aerosol-climate model ECHAM5-HAM. *Atmospheric Chemistry and Physics*, *5*(4), 1125–1156. https://doi.org/10.5194/acp-5-1125-2005

Tegen, I., Neubauer, D., Ferrachat, S., Siegenthaler-Le Drian, C., Bey, I., Schutgens, N., et al. (2019). The global aerosol–climate model ECHAM6.3–HAM2.3 – Part 1: Aerosol evaluation. *Geoscientific Model Development*, *12*(4), 1643–1677. https://doi.org/10.5194/gmd-12-1643-2019

Vogt, S., Herzog, G. F., & Reedy, R. C. (1990). Cosmogenic nuclides in extraterrestrial materials. *Reviews of Geophysics*, *28*(3), 253–275. https://doi.org/10.1029/RG028i003p00253

Wang, Q., Jacob, D. J., Fisher, J. A., Mao, J., Leibensperger, E. M., Carouge, C. C., et al. (2011). Sources of carbonaceous aerosols and deposited black carbon in the Arctic in winter-spring: Implications for radiative forcing. *Atmospheric Chemistry and Physics*, *11*(23), 12453–12473. https://doi.org/10.5194/acp-11-12453-2011

Wesely, M. L. (1989). Parameterization of surface resistances to gaseous dry deposition in regional-scale numerical models. *Atmospheric Environment*, *23*(6), 1293–1304. https://doi.org/10.1016/0004-6981(89)90153-4

Zhang, F., Wang, J., Baskaran, M., Zhong, Q., Wang, Y., Paatero, J., & Du, J. (2021). A global dataset of atmospheric ^{7}Be and ^{210}Pb measurements: Annual air concentration and depositional flux. *Earth System Science Data*, *13*(6), 2963–2994. https://doi.org/10.5194/essd-13-2963-2021

Zheng, M., Adolphi, F., Ferrachat, S., Mekhaldi, F., Lu, Z., Nilsson, A., et al. (2024). Modeling atmospheric transport of cosmogenic radionuclide ^{10}Be using GEOS-Chem 14.1.1 and ECHAM6.3-HAM2.3: Implications for solar and geomagnetic reconstructions [Dataset]. figshare. https://doi.org/10.6084/m9.figshare.24251884.v2

Zheng, M., Liu, H., Adolphi, F., Muscheler, R., Lu, Z., Wu, M., & Prisle, N. L. (2023). Simulations of ^{7}Be and ^{10}Be with the GEOS-Chem global model v14.0.2 using state-of-the-art production rates. *Geoscientific Model Development*, *16*(23), 7037–7057. https://doi.org/10.5194/gmd-16-7037-2023

Zheng, M., Sturevik-Storm, A., Nilsson, A., Adolphi, F., Aldahan, A., Possnert, G., & Muscheler, R. (2021). Geomagnetic dipole moment variations for the last glacial period inferred from cosmogenic radionuclides in Greenland ice cores via disentangling the climate and production signals. *Quaternary Science Reviews*, *258*, 106881. https://doi.org/10.1016/j.quascirev.2021.106881

References From the Supporting Information

Koldobskiy, S., Mekhaldi, F., Kovaltsov, G., & Usoskin, I. (2023). Multiproxy reconstructions of integral energy spectra for extreme solar particle events of 7176 BCE, 660 BCE, 775 CE, and 994 CE. *Journal of Geophysical Research: Space Physics*, *128*(3), e2022JA031186. https://doi.org/10.1029/2022JA031186

World Meteorological Organization. (1957). Meteorology—A three-dimensional science: Second session of the commission for aerology. *WMO Bull*, *4*, 134–138.